Proceedings of the 5th World Congress on Momentum, Heat and Mass Transfer (MHMT'20)
~~Lisbon, Portugal~~ Virtual Conference– October 2020
Paper No. ICMFHT 154
DOI: 10.11159/icmfht20.154

Flow Boiling of Water in Square Cross Section Microchannel at Different Inlet Subcooling Conditions

S. Korniliou[1], T. G. Karayiannis[2]
[1]National Physical Laboratory, Hampton Road, Teddington, Middlesex, TW11 0LW, UK
[2]Department of Mechanical and Aerospace Engineering, Brunel University London
Uxbridge UB8 3PH, UK
Sofia.Korniliou@npl.co.uk; Tassos.Karayiannis@brunel.ac.uk

Abstract **-** The effect of inlet subcooling on flow boiling heat transfer of deionised water in a horizontal single-microchannel of square cross section 1.0 mm by 1.0 mm and 75 mm long was studied. Three inlet sub-cooling conditions of 50, 15 and 5 K were studied for the mass fluxes of 200, 400 and 600 kg/m^{2}s with increasing base heat fluxes in the range of 105- 455 kW/m^2. Flow boiling patterns were related to corresponding local heat transfer coefficient along the microchannel and pressure drop characteristics for each inlet sub-cooling condition. This study demonstrates that, inlet sub-cooling has a significant effect on the two-phase heat transfer rates, pressure drop and flow patterns in the range studied.

Keywords**:** Flow boiling, Square Microchannel, Flow patterns, Heat transfer, Pressure Drop

1. Introduction

Despite the numerous experimental studies that have investigated flow boiling characteristics in microchannels there are still disagreements on the prevailing flow patterns, heat transfer rates and pressure drop trends, see Mahmoud and Karayiannis [1] and Cheng and Xia [2]. Among others and in relation to this work for example, there is no agreement on the dependence of heat transfer coefficient with heat flux. Past reports refer to a strong dependence of the heat transfer coefficient on heat flux. However, there is a number of studies that show no dependence of heat transfer coefficient with heat flux after a certain heat flux value value for small channels [3, 4]. It is therefore important to carry out experiments at different parameters and relate the heat transfer behaviour and pressure drop to the corresponding flow regimes in order to understand the heat transfer mechanisms and develop new prediction models [2]. Water, despite its high thermal conductivity and specific heat, has not been studied extensively. In this study, the local heat transfer coefficients at seven locations along the microchannel were acquired and related to flow pattern observations. The main objective of the present work was to investigate the heat transfer, flow patterns and pressure drop characteristics in a square metallic microchannel at different inlet subcooling, mass flux and heat flux conditions using deionised water.

2.1 Experimental Facility and Data Reduction

Fig. 1 depicts the experimental facility, which consists of a reservoir, sub-cooler, magnetic drive gear pump, Coriolis flow meter, preheater, inline filter, sight glass, test section, chiller, condenser and a high-speed camera (MicroLAB110 Phantom) coupled with a microscope. After degassing in the reservoir, DI water was circulated in the flow loop system at the desired flow rate and inlet temperature. The system pressure was maintained constant by controlling the reservoir temperature.

The test section assembly, depicted in Fig. 2 (a), consists of nine parts. A single rectangular microchannel 1 mm high, 1mm wide and 75 mm long was cut in the top surface of an oxygen free copper

block using a high-speed micro-milling machine (Kern HSPC 2216), see Fig. 2 (b). The average surface roughness (*Ra*) of the microchannel was measured at five locations of the channel bottom and was found to be 0.252 ± 0.08 μm. The inlet and outlet plenums of the test section were fabricated in polycarbonate in order to reduce the heat transfer losses. Seven K-type calibrated thermocouples (accuracy of ± 0.12 K) were inserted into the copper block at a distance of t=0.7 mm below the channel bottom to obtain surface temperatures along the channel (see Fig. 2 (c)). Readings from thermocouples T9, T11, T12, and T13 where used to evaluate the heat flux in the copper block and thermocouples T8-T10 to evaluate the temperature distribution in the horizontal direction of the copper block. Two cartridge heaters, total 1000 W, were placed horizontally, parallel to the channel inside the copper block. A borosilicate glass cover plate was used on top of the microchannel to allow flow visualization, supported in place by an aluminum cover and bottom plate. The inlet pressure was measured at the inlet plenum using an absolute pressure transducer. The pressure drop between the microchannel inlet and outlet was measured using a differential pressure transducer. Inlet and outlet liquid temperatures were measured using two K-type thermocouples. Flow visualisation was carried out along the microchannel at a frame rate of 4,609 fps and resolution of 768 x 480 pixels. The flow boiling experiments were carried out at different subcooling conditions of ΔT_{sub} = 5, 15 and 50 K for the base heat fluxes in the range of 105-455 kW/m^2 at three constant mass fluxes of 200, 400 and 600 kg/m^{2}s and pressure of 1.05 ± 0.05 bar measured at the channel inlet. The experimental setup was validated with single-phase experiments. The single-phase fanning friction factor (f_{exp}) was calculated as:

$$f_{exp} = \frac{\rho_l D_h \Delta P_{ch}}{2 L_{ch} {G_{ch}}^2} \tag{1}$$

where ρ_l is the liquid density, G_{ch} is the mass flux, D_h the hydraulic diameter, L_{ch} is the channel length and

ΔP_{ch} the channel pressure drop calculated using Eq. (2):

$$\Delta P_{ch} = \Delta P_{meas} - \Delta P_{loss} \tag{2}$$

ΔP_{meas} is the overall measured pressure drop between the channel inlet and outlet plenums and ΔP_{loss} is the pressure loss due to the change of flow direction, sudden contraction and expansion due to the plenums:

$$\Delta P_{loss} = 2 * \left(\frac{1}{2} K_{90} G_{pl}^2 v_l\right) + \frac{1}{2} K_{90} G_{pl}^2 v_l \left\{[1 - (a^2) + 0.5(1-a)] + \left[\frac{1}{a^2} - 1 + (1-a)^2\right]\right\} \tag{3}$$

where a is the ratio of minimum to maximum cross sectional area, G_{pl} is the plenum mass flux, v_l the liquid specific volume and K_{90} is the loss coefficient due to 90° turns [5]. The base heat flux was calculated from:

$$q^{"} = -k_{cu} \frac{dT}{dy} \tag{4}$$

where k_{cu} the thermal conductivity of copper and $\frac{dT}{dy}$the temperature gradient along the vertical direction of the copper block.

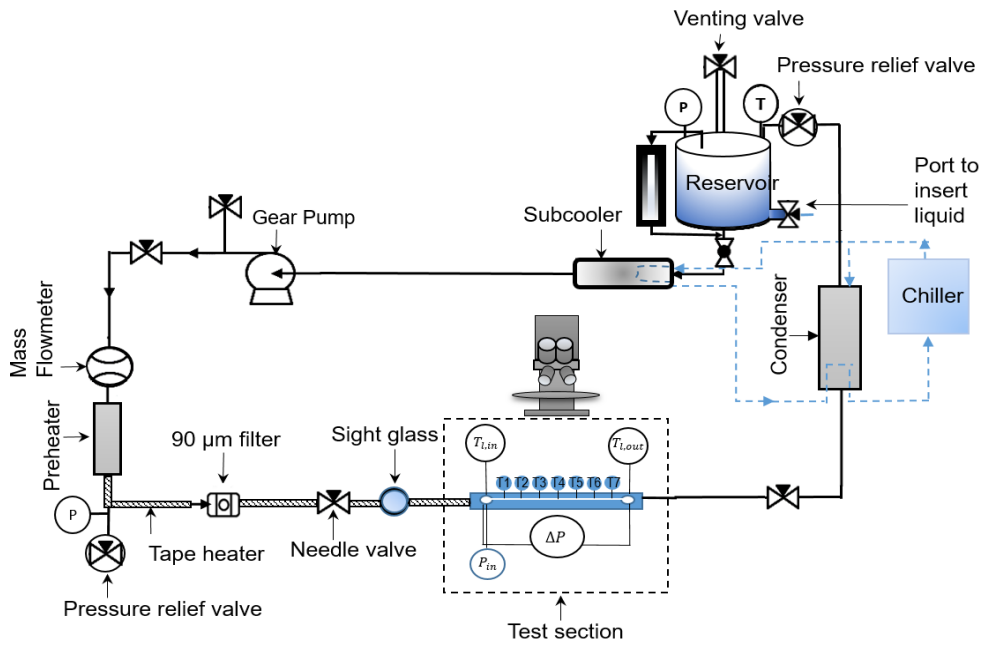

Fig. 1: Experimental test rig.

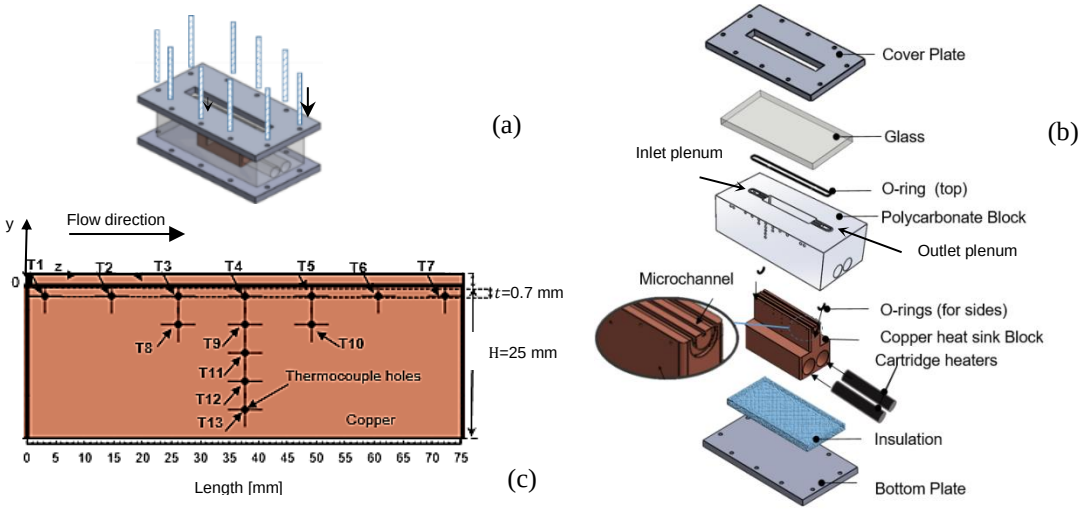

Fig. 2: Final test assembly (a), test section parts (b) and side view of the copper block (c).

The channel base temperature was estimated by adopting the 1D assumption using the equation bellow:

$$T_w(z) = T(z) - \frac{q^{"} t}{k_{cu}} \tag{5}$$

where $T(z)$ is the local temperature measured using thermocouples at t= 0.70 mm below the channel base. The local fluid temperature was estimated from:

$$T_f(z) = T_i - \frac{q^{"} W z}{\dot{m} c_p} \tag{6}$$

where T_i is the inlet liquid temperature, $W$is the channel width, z is the axial distance, $\dot{m}$ the measured mass flow rate and c_p the specific heat capacity.

The local single-phase heat transfer coefficient (h_{sp} (z)) and average Nusselt number (Nu) were calculated as:

$$h_{sp}(z) = \frac{q^{"}}{T_w(z) - T_f(z)} \tag{7}$$

$$Nu = \frac{1}{L_{ch}} \int_0^L \frac{h_{sp}(z) D_h}{k_l} dz \tag{8}$$

where k_l is the thermal conductivity of water.
The single-phase region starts from the channel inlet to the location of zero thermodynamic quality with length L_{sub}, calculated interactively from Eqs. (9)- (11):

$$L_{sub} = \frac{\dot{m} c_p (T_{sat} - T_i)}{q^{"}(2W + H)} \tag{9}$$

$$P_{sat}(L_{sub}) = P_i - \Delta P_{sp} \tag{10}$$

$$\Delta P_{sp} = \frac{2 f_{app}}{\rho_l D_h} L_{sub} \tag{11}$$

where T_{sat} is the liquid saturation temperature, P_i is the inlet pressure, H the channel height and f_{app} is the apparent friction factor calculated from Shah [6] using the following equations :

$$f_{app} = \frac{3.44}{Re\sqrt{L_{sub}^{*}}} + \frac{(f_{FD}Re) + \frac{K(\infty)}{4L_{sub}^{*}} - \frac{3.44}{\sqrt{L_{sub}^{*}}}}{Re[1 + C(L_{sub}^{*})^{-2}]} \tag{12}$$

$$L_{sub}^{*} = \frac{L_{sub}}{ReD_h} \tag{13}$$

$$f_{FD}Re = 24(1 - 1.3553\beta + 1.9467\beta^2 - 1.7012\beta^3 + 0.9564\beta^4 - 0.2537\beta^5) \tag{14}$$

where β is the aspect ratio of the channel ($\beta = W/H$) and the values of constants $C = 0.0021$ and $K(\infty) = 1.28$ are given in Shah [6] for rectangular channel.

The local two-phase heat transfer coefficient is calculated from the following equation:

$$h_{tp}(z) = \frac{q^{"}}{(T_w(z) - T_{sat}(z))} \tag{15}$$

The local saturation temperature $T_{sat}(z)$ was calculated from the local pressure in the two-phase region by assuming linear pressure drop along the channel.

The local vapour quality was calculated from Eqs. (16-17) :

$$x(z) = \frac{i(z) - i_i(z)}{i_{lg}(z)} \tag{16}$$

$$i(z) = i_i + q^{"} \frac{(2H + W)z}{\dot{m}} \tag{17}$$

where $i(z)$ is the local liquid specific enthalpy, $i_i(z)$ is the local inlet specific enthalpy and $i_{lg}(z)$ is local enthalpy of vaporisation.

Experimental uncertainties were calculated based on the method described by Coleman and Steele [7]. The maximum experimental uncertainty in the flow rate, heat flux, heat transfer coefficient and

pressure drop calculation was 9.6%, 15 %, 13% and 7 %. The uncertainty for the heat flux was found to decrease with an increase in heat flux and/or mass flux.

2.2 Validation of experimental facility

Fig. 3 (a) shows experimental and predicted single-phase friction factor versus Reynolds number (Re). The relationship for the theoretical friction factor for laminar developing flow of non-circular channel is given by Shah and London [8] and predicted the experimental data well with a Mean Absolute Error (MAE) of 2.8-12.3 %. Fig. 3 (b) shows single phase average Nusselt number as a function of Re, which compared well with the correlation of Shah and London [9] for developing flow, for the range of mass fluxes between 200-1950 kg/m^{2}s and for Re <2000, i.e. MAE of 2.03-8.00 %.

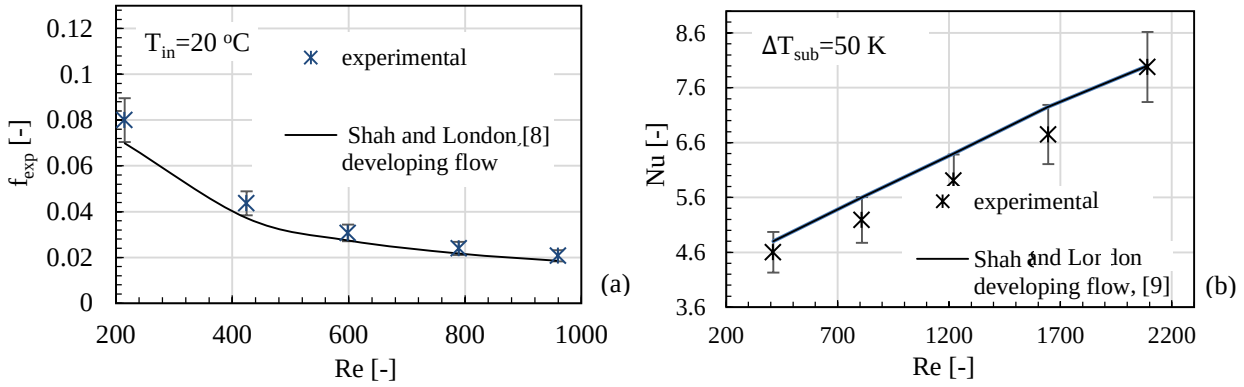

Fig. 3: Experimental and theoretical single-phase friction factor (a) and average Nu number (b) versus Re.

The temperature variation in the axial direction, between thermocouples T8, T9 and T10 for both single-phase and two-phase regimes was very small (< 0.6 K). Therefore, heat flux was considered uniform at the channel base. The reproducibility of the experiments is presented in Fig. 4 where the averaged heat transfer coefficient data obtained at two different days are compared for the same mass flux of 200 kg/m^{2}s, heat flux range from 82 to 455 kW/m^2 and inlet sub-cooling of ΔT_{sub} = 5 K. As seen in the figure, the data were reproducible and within the experimental uncertainty.

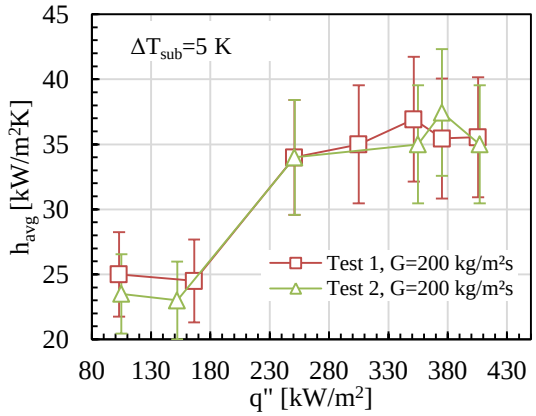

Fig. 4: Average heat transfer coefficient at two different days at 200 kg/m^{2}s and ΔT_{sub}= 5 K as a function of increasing heat flux.

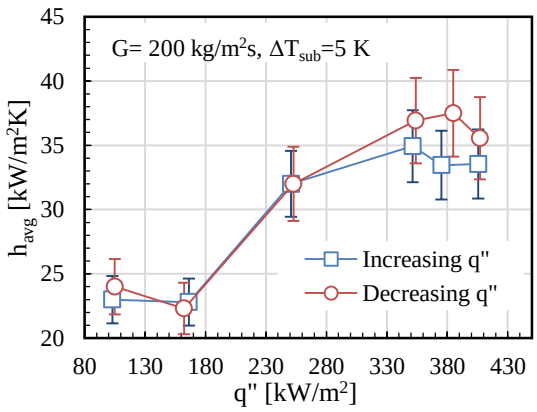

Fig. 5: Average heat transfer coefficient results for increasing and decreasing heat flux for the mass flux of 200 kg/m^{2}s at ΔT_{sub}=5 K.

Fig. 5 shows the respective averaged heat transfer coefficient for the mass flux of 200 kg/m^{2}s at increasing and decreasing heat flux, for inlet subcooling of ΔT_{sub} = 5 K. In the case of decreasing heat flux, averaged heat transfer coefficient was measured 5 % higher in the two-phase region compared to the case of increasing heat flux. The variation was found to be within the experimental uncertainty. Maximum variation of 8 % was measured for case of the highest mass flux of 600 kg/m^{2}s.

3. Results and Discussion

3.1 Flow patterns

The main flow patterns observed in this study were bubbly (B), confined bubble (CB), slug (S), elongated slug (ES), churn (C) and annular flow (A), see fig. 6. These flow regimes were not stable, but they were alternating with time for each single location. The annular flow, seen at the start of the channel, was elongated slug with local dry-out in the film. Bubble nucleation in the thin film of annular flow was also observed. Fig. 6 shows instants of the periodic two-phase flow patterns along the first 10 mm from the entry, for ΔT_{sub}=50 K at the mass flux value of G =200 kg/m^{2}s and heat flux of q''=255 kW/m^2 for one cycle period of 2.8 s. At the beginning of the cycle (t=0 s) fresh liquid enters the channel and churn flow is observed. Then, bubbly flow occurs at t=0.2 s for a very short distance from the channel entry (first 10 mm) and short time. The bubbles were observed to reach channel dimensions very quickly (confined bubble flow regime) at t= 0.4 s, at a very short distance from the channel inlet (0.8 mm). Then the confined bubbles coalescence with smaller bubbles forming slugs. Therefore, the bubbly flow turned to slug flow very early along the channel (t= 0.5 s).

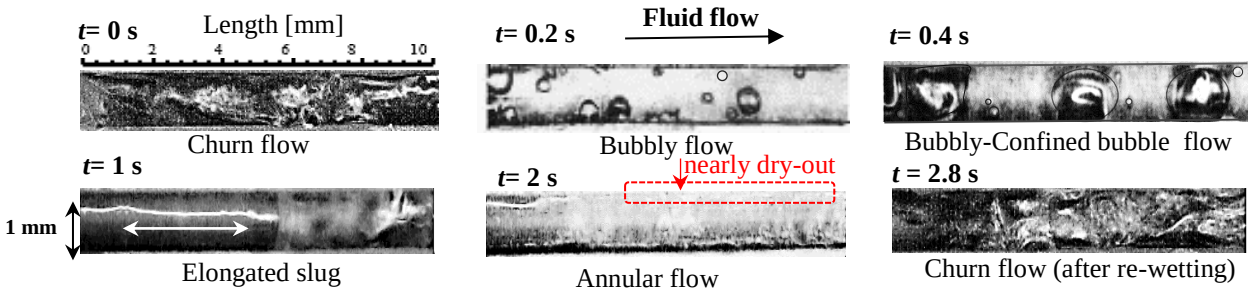

Fig. 6: Instants of alternating flow patterns at 10 mm from the channel entry, for a constant heat flux of q''=255 kW/m², lowest mass flux of of G =200 kg/m^{2}s at high inlet sub-cooling of ΔT_{sub}= 50 K.

Flow reversal was observed to occur due to rapid growth of the elongated slug at t=1 s to both directions. This stage appears to be driven by intense evaporation from the bottom and the sides of the channel. Flow reversal was observed at almost all heat fluxes greater than 155 kW/m^2. This resulted in flow instabilities and fluctuations in pressure drop and fluid and wall temperatures. For example, the inlet fluid temperature varied up to 6 K and the induced pressure drop fluctuations with an amplitude of up to 5 kPa as the heat flux increased up to 385 kW/m^2.Finally, annular-like flow regime was established at t=2.0 s with decreasing thin film along the length. Instants of the flow patterns were captured at all channel locations. When nearly dry-out state was reached, re-wetting occurred at t=2.8 s, followed by repeat of this cycle of events at roughly 2.8 s. Churn flow was observed to occur only at a very small section of the channel during re-wetting. For low sub-cooling of ΔT_{sub}=5 K at the same G and q''as in fig.6, bubble flow was not observed. Bubble nucleation and growth in the liquid film of annular flow established further downstream was clearly observed. The discussed flow regimes were also observed in small channels by Kingston *et* al. [10], Kandlikar and Steinke [11] and Diaz and Schmidt [4], using HFE 7100, water and n-hexane respectively.

3.2 Two-Phase Pressure Drop

Two-phase pressure drop increased with increasing heat flux after boiling incipience for all the tested mass fluxes. Fig. 7 shows the effect of heat flux on two–phase pressure drop of the channel for the mass flux of 200 kg /m^{2}s at ΔT_{sub} =50 K and 5 K. Increase in two-phase pressure drop with heat flux occurred due to increase in vapour generation and therefore increase in acceleration pressure drop component [10]. Decreasing the inlet sub-cooling for the same mass flux, resulted in higher two-phase pressure drop for all the mass fluxes. At high heat flux values (≥ 340 kW/m^2) the curves converge to the same values indicating that similar flow patterns prevail for most of the channel length for both degrees of subcooling.

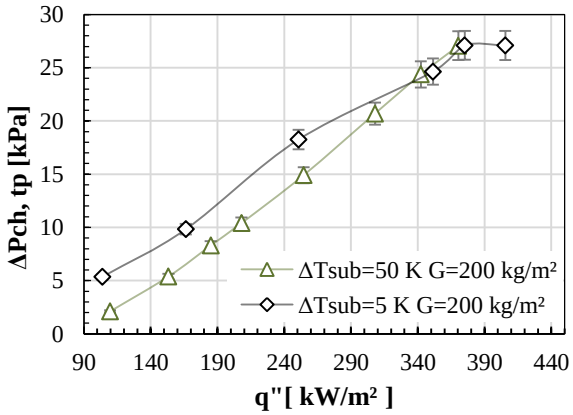

Fig. 7: Two-phase pressure drop as a function of heat flux for G=200 kg/m^{2}s at ΔT_{sub}=50 K and ΔT_{sub}=5 K.

3.3 Local heat transfer coefficient

Figs. 8 (a) and 8 (b) present the local heat transfer coefficient (h_{local}) as a function of local vapour quality for the mass flux of G=200 kg/m^{2}s, for the heat fluxes of 105, 155, 255 and 355 kW/m^2 at ΔT_{sub}= 5 K and ΔT_{sub}=50 K, respectively. The corresponding most dominant flow patterns are marked on each figure. The effect of sub-cooling is obvious for all q". Decreasing sub-cooling results in higher heat transfer coefficient for the same mass flux and heat flux condition.

The heat transfer coefficient increases with increasing heat flux up to 255 kW/m^2 for both ΔT_{sub}= 5 and 50 K. Increasing further the heat flux resulted in a reduction in the heat transfer coefficient. The decrease of the two-phase heat transfer coefficient with increase of heat flux for heat fluxes higher than 340 kW/m^2 was also found by Özdemir *et* al. [3] in a 1 mm by 0.3 mm copper microchannel using water for G=208 kg/m^{2}s, at vapour qualities higher than 0.3. They identified temperature and pressure fluctuations resulting from temporal flow reversal and they attributed the decrease of two phase heat transfer coefficient to the suppression of nucleate boiling and the formation of dry patches beneath the elongated bubble.

The heat transfer coefficient exhibited a decreasing trend with local vapour quality in the saturated region. Diaz and Schmidt [4] using n-hexane in a 0.3 mm by 12.7 mm and 200 mm length rectangular channel found that the local heat transfer coefficient decreased with quality after the quality reached zero. At high qualities the two-phase heat transfer coefficient is almost independent of quality. Qu and Mudawar [12] in a study with water for a heat sink of rectangular microchannels also found that the heat transfer coefficient decreases with vapour quality. The same group, Lee and Mudawar [13] also found a similar trend for a heat sink (203.2 x 609.6 mm) with 100 of 1 x 1 mm flow channels using R134a.

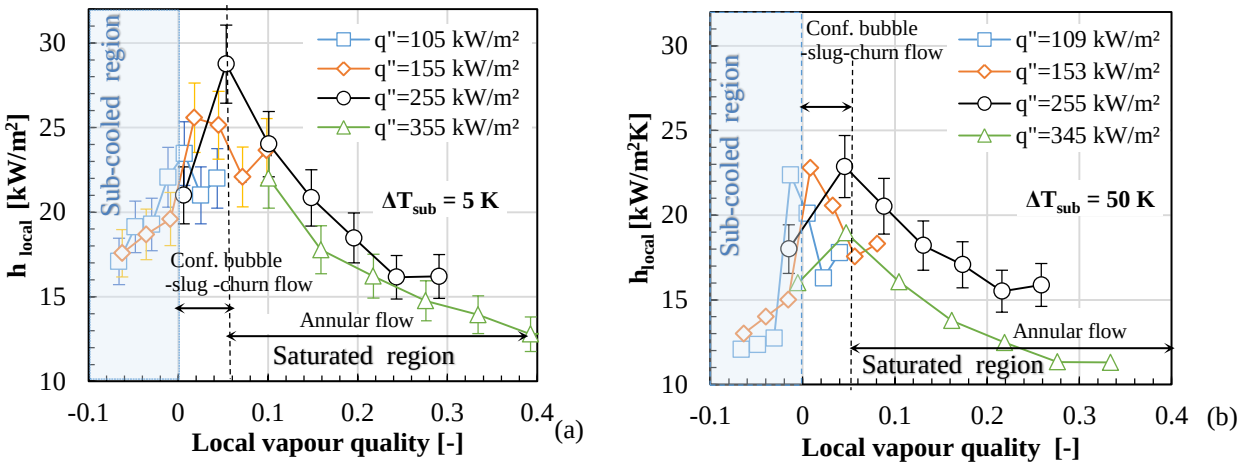

Fig. 8: Local heat transfer coefficient as a function of vapour quality for G=200 kg/m^{2}s and q"=105, 155, 255, 355 kW/m^2 at (a) low sub-cooling of ΔT_{sub}=5 K and (b) high sub-cooling of ΔT_{sub}= 50 K.

They explained the decrease by producing a model that considered initial droplet entrainment at the onset of annular flow as well as droplet deposition along the channel, which resulted in liquid film thickening during annular flow, following with a decrease in the local heat transfer coefficient. They found this trend for the heat fluxes in the range of 10.0 to 26.0 kW/m^2 and constant mass flux of G=208 kg/m^{2}s. However, there was no good agreement between the experimental two-phase heat transfer coefficients and the theoretical values. The trend of decreasing heat transfer coefficient with increasing local vapour quality of parallel microchannels with water was also found by Steinke and Kandlikar [11] and was attributed to flow reversal due to fast bubble growth leading to dry-out condition.

4. Conclusions

Flow boiling of water in a single microchannel was conducted at different operating conditions to study flow patterns, pressure drop and heat transfer rates at different inlet subcooling values. Transient two-phase flow regimes were observed such as bubbly, confined bubble-slug, churn, annular flow; and annular flow with bubbles in the liquid film. Temporal flow reversal caused by rapid bubble growth, was observed to occur at heat fluxes >255 kW/m^2. This caused near dry-out conditions at certain locations in the channel. Bubbly-confined bubble and slug flow occurred for longer length of the channel at low mass flux compared to high mass flux. At low-subcooling, the single-phase region was almost absent, bubbly flow was supressed due to the confinement effect and annular flow dominated the channel at all mass fluxes and high heat fluxes.

Two-phase pressure drop reached the higher values for the low inlet subcooling case for all mass fluxes, due to the longer two-phase length. The values converged at high heat fluxes.

Low sub-cooling resulted in higher local two-phase heat transfer coefficients for heat fluxes lower than 255 kW/m^2. Increasing the heat flux further, during saturated flow boiling resulted in a decrease of the two-phase local heat transfer coefficient for both sub-cooling conditions. At high heat fluxes, flow reversal due to bubble confinement resulted in temporal nearly dry-out and therefore h_{tp} early deterioration, which may explain the drop of the heat transfer coefficient. The trend of decreasing two-phase heat transfer coefficient with local vapour quality could be attributed to the occurrence of nearly dry-out local regions.

Acknowledgement

The contribution and comments of Dr M. Mahmoud are gratefully acknowledged.

References

[1] M. M. Mahmood and T. G. Karayiannis, "Chapter 4: Flow Boiling in Mini to Microdiameter Channels," in *Encyclopedia of Two-Phase Heat Transfer and Flow IV*, pp. 233–301, 2018.

[2] L. Cheng and G. Xia, "Fundamental issues, mechanisms and models of flow boiling heat transfer in microscale channels," *Int. J. Heat Mass Transfer*, vol. 108, pp. 97-127, 2017.

[3] M.R. Özdemir, M.M.Mahmood and T.G. Karayiannis, "Flow boiling heat transfer in a rectangular copper microchannel," *J. Therm. Eng.*, vol. 2, no. 2, pp. 761–773, 2016.

[4] Diaz M.C. and Schmidt J.,"Flow boiling of n-hexane in small channels: heat transfer measurements and flow pattern observations ", *Chem. Eng. Technol*., 30 , No.3, pp. 389-394, 2007.

[5] R. J. Phillips, "Forced convection, liquid-cooled, microchannel heat sinks", *Cambridge, M.I.T., M.Sc.Thesis*, 1987.

[6] R. K. Shah, "Correlation for Laminar Hydrodynamic Entry Length Solutions For Circular And Noncircular Ducts", *J. Fluids Eng. Trans.* ASME, 1978.

[7] H.W. Coleman and W.G. Steele, "Experimentation and Uncertainty Analysis for Engineers", Wiley, 1999.

[8] R. K. Shah and A. L. London, "Advances in Heat Transfer: Laminar Flow Forced Convection in Ducts Suppt. 1," in *Laminar Flow Forced Convection in Ducts*, 1978.

[9] R. K. Shah and A. London, "Laminar flow forced convection in ducts : a source book for compact heat exchanger analytical data", *Academic Press*, 1978.

[10] T. A. Kingston, J. A. Weibel, and S. V. Garimella, "High-frequency thermal-fluidic characterization of dynamic microchannel flow boiling instabilities: Part 2 – Impact of operating conditions on instability type and severity," *Int. J. Multiphase Flow*, vol.106, pp.189-201, 2018.

[11] M. E. Steinke and S. G. Kandlikar, "An experimental investigation of flow boiling characteristics of water in parallel microchannels," J. Heat Transfer, vol. 126, no. 4, p. 518, 2004.

[12] W. Qu and I. Mudawar, "Flow boiling heat transfer in two-phase micro-channel heat sinks—II. Annular two-phase flow model," *Int. J. Heat Mass Transfer*, vol. 46, no. 15, pp. 2773–2784, 2003.

[13] S. Lee and I. Mudawar, "Enhanced model for annular flow in micro-channel heat sinks, including effects of droplet entrainment/deposition and core turbulence," *Int. J. Heat Mass Transfer*, vol.133, pp.510-530, 2019.